

Human Iridal Stroma Melanosomes of Varying Pheomelanin Contents Possess a Common Eumelanic Outer Surface

Dana N. Peles,[†] Lian Hong,[†] Dan-Ning Hu,[‡] Shosuke Ito,[§] Robert J. Nemanich,[#] and John D. Simon^{*,†}

Department of Chemistry, Duke University, Durham, North Carolina 27708, Tissue Culture Center, The New York Eye and Ear Infirmary, New York Medical College, New York, New York 10003, Department of Chemistry, Fujita Health University School of Health Sciences, Toyoake, Aichi 470-1192, Japan, and Department of Physics, Arizona State University, Tempe, Arizona 85287-1504

Received: May 4, 2009; Revised Manuscript Received: July 1, 2009

Uveal melanosomes originating in the iridal stroma contain both black (eumelanin) and red (pheomelanin) pigment. Recent studies reveal that the eumelanin/pheomelanin ratio varies with iris color, with lower ratios being observed for lighter color (hazel, blue) irides. This is of great interest because the epidemiology of uveal melanomas also indicates an increased incidence for lighter-colored irides. Herein, we examine human iridal stroma melanosomes from dark brown and blue–green irides, which are characterized by a eumelanin/pheomelanin ratio of 14.8 and 1.3, respectively. Atomic force microscopy reveals that the melanosomes extracted from these different colored irides have a similar size and overall morphology. Studies of the surface ionization potentials reveal that the surface of these melanosomes is pure eumelanin, despite the significant difference in their overall pigment composition. These data indicate that the pheomelanin present in the melanosome is encased by eumelanin, providing support for the “casing model” architecture of mixed melanins advanced from kinetic studies of the early steps in the melanogenesis pathway. Because of the different bulk composition, these results indicate that the thickness of the outer eumelanin coating decreases as the iride color lightens. Oxidative damage to the melanosome surface is therefore more likely to enable access to the photoreactive pheomelanin in the lighter irides than that in the eumelanin-rich dark irides. This provides new insights into the potential contribution of iridal stroma melanosomes both to inducing oxidative stress and to accounting for the observed iris-color-dependent epidemiology of uveal melanoma.

Introduction

Melanin is a naturally occurring pigment found throughout the eye, hair, inner ear, and skin of the human body. The pigment is categorized into two groups described by color and molecular precursor, eumelanin (black–brown) and pheomelanin (red–yellow). In situ, mixtures of both pigments are produced within specialized organelles termed melanosomes. However, the resulting ratio varies^{1–3} and is subsequently discussed as a biologically significant marker.^{3–6} More specifically, this ratio has been discussed in relation to the epidemiological data for skin cancer rates, indicating an observed increased incidence for increased relative concentrations of pheomelanin.^{5,6} Recent studies suggest that a similar trend exists underlying the epidemiology of uveal melanoma,^{3,4} the most common intraocular malignant tumor in human adults. Thus, characterization of the photoreactivity of melanosomes with variable eumelanin/pheomelanin ratios is critical to understanding the function and the possible contributions they may play in the molecular mechanisms underlying these melanomas.

Cutaneous and uveal (iridal, ciliary, and choroidal) melanocytes, cells that synthesize melanosomes, are both of neural crest origin,⁷ and furthermore, the initial steps of the melanogenesis for eumelanin and pheomelanin deposited within both of these

melanosomes is described with the Raper–Mason–Prota scheme.⁸ Initiation of both pigment processes is achieved only after the formation of dopaquinone by the tyrosinase oxidation of tyrosine or 3,4-dihydroxyphenylalanine (dopa). Eumelanin is mostly produced from the molecules 5,6-dihydroxyindole and 5,6-dihydroxyindole-2-carboxylic acid, which form with the subsequent reactions of dopaquinone. The molecular components of pheomelanin, however, are the benzothiozine units formed from the subsequent oxidation of cysteinyl-dopa. Contrary to eumelanin, the formation of pheomelanin is only accomplished if sulfur-containing compounds, for example, cysteine, are present. In vitro kinetic studies associated with the initial biosynthetic steps have been conducted to provide data on the rates of formation of pheomelanin versus that of eumelanin.^{9,10} These efforts indicate that pheomelanin production is dominant as long as sulfhydryl compounds are present in the system. Upon depletion of these compounds, eumelanin formation prevails. Results from these kinetic models suggest that the surface of a mixed melanic pigment is eumelanic with a pheomelanic core.^{8,11} This type of molecular structure has been previously proposed based on biochemical studies of mixed melanogenesis and solubility properties of synthetic model systems.^{12,13} This model has been verified for neuromelanin granules,^{14,15} but the precursors for the human brain pigment differ from those that generate the pigment found in cutaneous and uveal melanins.¹⁶

Despite the compelling evidence presented from the in vitro studies, direct evidence supporting a “casing model” architecture for mixed melanic melanosomes isolated from the skin or uvea

* To whom correspondence should be addressed. E-mail: john.simon@duke.edu.

[†] Duke University.

[‡] New York Medical College.

[§] Fujita Health University School of Health Sciences.

[#] Arizona State University.

has not been reported. Yet, as the surface of the melanosome is central to its function(s),¹⁷ elucidation of the pigment composition of the surface is necessary. Photoprotection is usually discussed as a function of melanosomes, especially in cutaneous and uveal melanosomes, as they absorb UV radiation under normal solar illumination.^{4,17} Accompanying this absorption, however, is the possible generation of photoexcited reactive oxygen species (ROS) that can be detrimental to the cell.^{18,19} The photoprotective and potentially deleterious side effects of photoinduced oxidative stress is a result of the photoreactivity of the two pigments. Eumelanin is generally identified as photoprotective and antioxidant, whereas pheomelanin is generally identified as photoreactive and pro-oxidant.^{20–24} Thus, the composition of the surface pigment(s) may provide insight into the balance of this duality and the possible roles melanosomes may play in the molecular mechanisms of cutaneous and uveal melanoma.

Photoemission electron microscopy (PEEM) is a unique, surface-sensitive imaging technique capable of differentiating between eumelanin and pheomelanin.^{20,25,26} As a surface-sensitive tool that probes a characteristic property of the sample (photoionization threshold), the composition of the surface of the melanosome can be investigated. Herein, we use PEEM to study the surface electrochemical properties of iridal stroma melanosomes. These melanosomes, isolated from different colored irides, have different distributions of eumelanin/pheomelanin ratios.^{3,27} This affords us the opportunity to investigate the surface photoreactivity as the relative pheomelanin concentration changes.

Experimental Section

Sample Isolation. Extraction of the iris was performed on donor eyes from two patients of different colors and ages, dark brown, age 14, and blue–green, age 66. The posterior iridal pigment epithelium (IPE) was isolated from the iris with a previously described method,²⁷ and the remaining IPE-scraped iris tissues were stored at $-70\text{ }^{\circ}\text{C}$ until further use. An enzymatic extraction was used to isolate the iridal stroma melanosomes from the iris tissue using the same procedure as that reported on melanosome isolation from bovine iris.²⁸ Briefly, wet iris tissue was cut into small pieces and subjected to three steps of enzyme digestions at $37\text{ }^{\circ}\text{C}$ in PBS under argon, collagenase (68 U/mL, with 2 mM CaCl_2) for ~ 16 h, pancreatin (2.5 mg/mL) for 2 h, and trypsin (646 U/mL, with 2 mM CaCl_2) for 2 h. After each digestion, the remaining material was washed with water several times and then subsequently subjected to further enzyme digestions. Following these treatments, the materials were suspended in 1% (wt/vol) Triton X-100 solution and stirred for 1.5 h at room temperature under argon. The particles were then washed with methanol/water 1:1 (vol/vol) once and then with water four times. Afterward, the pellets were treated with collagenase (68 U/mL, with 2 mM CaCl_2) for 16 h at $37\text{ }^{\circ}\text{C}$ under argon. The resulting black to brown melanosomes were washed with water five times and kept at $-70\text{ }^{\circ}\text{C}$ until use.

Scanning Electron Microscopy. Melanosomes were suspended in a water suspension and dropped onto freshly cleaved mica slides in $2\text{ }\mu\text{L}$ aliquots. The slides were then mounted on stainless steel pegs with double stick tape and air-dried in the dark. The mounted samples were coated with Au/Pd under argon plasma for 2 min at 15 mA using a Hummer V sputter coater (Anatech, Springfield, VA). A Philips XL30 ESEM (FEI company, Hillsboro, OR) equipped with a backscattering secondary electron detector was used to examine the samples

in high vacuum mode. Multiple SEM images were captured at magnifications of $10\,000\times$ for each of the different samples. Care was taken to ensure that each image collected covered a completely different surface area. The dimensions of the melanosomes captured in the SEM images were measured using Scandium Imaging Software (Olympus Soft Image Solutions, Lakewood, CO). For each sample, over 1500 granules were measured from 6 to 14 images taken at $10000\times$ magnification. The histograms of the lengths of the short and long axes of the measured melanosomes were plotted and fit to a single Gaussian function.

Free Electron Laser Photoemission Electron Microscopy.

Details of the Elmitec ultrahigh vacuum PEEM and the Duke University FEL have been described previously.²⁹ Sample preparation was initiated by cleaving wafers of $\langle 100 \rangle$ -oriented silicon (N-type, P-doped) to square regions of approximately 1 cm^2 . These wafers were cleaned using the standard RCA wet chemical procedure³⁰ without the hydrofluoric acid step. Isolated iridal stroma melanosomes were suspended in a Nanopure water solution and deposited onto the cleaned silicon wafers in a $0.5\text{ }\mu\text{L}$ aliquot. The samples were allowed to air-dry in a sterile Petri dish before experimentation, and care was taken to avoid sample exposure to ultraviolet light. After drying (< 1 h), the samples were transferred under ultrahigh vacuum into the PEEM chamber for data collection. To ensure a large sampling, the instrumental field of view was set at $50\text{ }\mu\text{m}$. During experimentation, the FEL was tuned within a spectral region of $240\text{--}310\text{ nm}$ ($5.17\text{--}4.00\text{ eV}$) in 5 nm increments. After passing through a series of electron optics, the emitted electrons were magnified with a microchannel plate and subsequently imaged with a fluorescent screen. The intensity of the emitted photoelectrons was then acquired. All images were captured with a DVC-1312 M digital camera from DVC Company, Inc. (Austin, TX). The digital camera resolution was 1300×1030 pixels \times 12 bits. Acquisition times were 9 s.

Details of the FEL-PEEM image analysis have also been previously reported.^{20,26} For each wavelength analyzed in the FEL scan, an image was acquired and saved with the DVCView program. During acquisition, an appropriate software gain value and a multichannel plate voltage were selected to prevent image saturation. The wavelength-dependent integrated brightness, $S(\lambda)$, was subsequently determined from the CCD images and was taken to be proportional to the photocurrent collected. The resulting value was normalized for the software gain and the incident photon flux at each wavelength. Plotting $S(\lambda)$ versus the excitation energy, $h\nu$, produces a photoionization threshold curve, and when considering the temperature-related effects, the plot should satisfy the following equation³¹

$$S(\lambda) = T^2 f\left(\frac{h\nu - \chi}{k_B T}\right) \quad (1)$$

In this equation, T is temperature, k_B is the Boltzmann constant, χ is the photoionization threshold, $h\nu$ is the photon energy, and

$$\begin{aligned} f(u) &= e^u - \frac{e^{2u}}{2^2} + \frac{e^{3u}}{3^2} - \dots \quad (u \leq 0) \\ &= \frac{\pi^2}{6} + \frac{1}{2}u^2 - \left[e^{-u} - \frac{e^{-2u}}{2^2} + \frac{e^{-3u}}{3^2} - \dots \right] \quad (u \geq 0) \end{aligned}$$

The threshold of a sample is determined by functionally fitting the curves of $S(\lambda)/T^2$ versus $h\nu/k_B T$ with eq 1. IGOR Pro

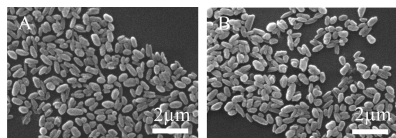


Figure 1. SEM images of (A) dark brown iris melanosomes and (B) blue-green iris melanosomes.

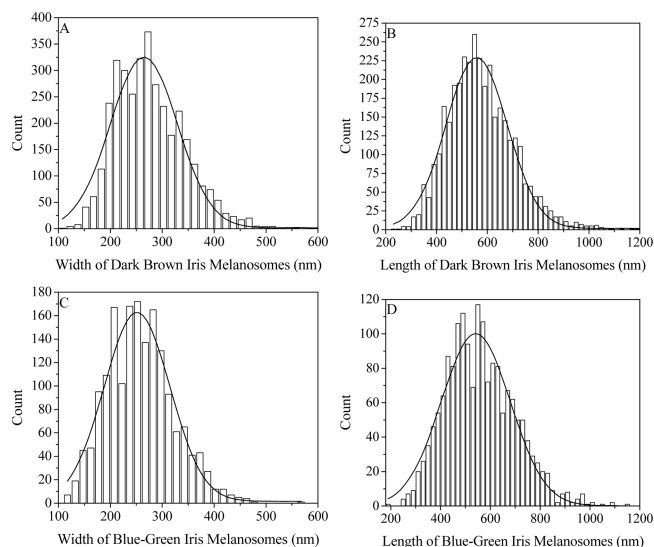


Figure 2. The resulting histograms for the length and width of dark brown iris melanosomes (A, B) and blue-green iris melanosomes (C, D). As shown, the distribution of lengths of the long and short axes are represented by single Gaussian distributions.

software (WaveMetrics, Lake Oswego, OR) was used to fit the normalized data.

Atomic Force Microscopy. A water suspension of iridal stroma melanosomes was pipetted in 0.5 μL aliquots onto freshly cleaved mica and allowed to air-dry in the dark. The instrument and method of imaging has been previously described in detail.³² Briefly, AFM height and phase images were collected with a NanoScope IIIa BioScope AFM (Digital Instruments, Santa Barbara, CA) operated in tapping mode. The AFM head was mounted on a Zeiss (Thornwood, NY) Axiovert S100 TV inverted optical microscope, allowing visual observation of the sample.

Results

Shape and Size Analysis of Iridal Stroma Melanosomes. SEM imaging was used to analyze the morphology of blue-green and dark brown iridal stroma melanosomes from donors of age 66 and 14, respectively (Figure 1). The shape and size observed in the analysis revealed a consistent morphological distribution across samples regardless of their respective age or iris color origins. The long and short axes of the melanosomes were measured from these images, and the resulting histograms were fit to a single Gaussian function (Figure 2). The outcomes of the fitting are given in Table 1. The morphology revealed for these iridal stroma melanosomes by SEM is in agreement with previously reported morphological results on iridal stroma melanosomes by transmission electron microscopy (TEM).^{33,34}

Surface Photoionization Potentials of Iridal Stroma Melanosomes. The surface composition of melanosomes isolated from iridal stroma tissue was examined using FEL-PEEM. Melanosomes isolated from dark brown and blue-green irides were analyzed. The integrated intensity (S) of the PEEM images was determined as a function of the excitation wavelength

TABLE 1: Summary of the Size Analysis of the Melanosomes Isolated from Human Irises^a

iris color	length/nm	width/nm
dark brown	560 (140)	260 (80)
blue-green	540 (160)	250 (70)

^a The error in measuring the dimension is <5%. The histograms of the lengths of both the long and short axes were fit to a single Gaussian function. The peak of the distribution is tabulated. The half-width of the distribution is given in parentheses.

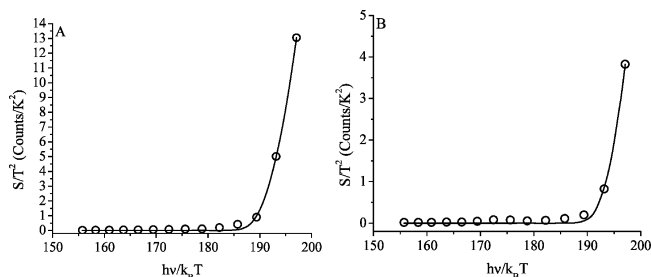


Figure 3. Wavelength-dependent FEL-PEEM data plotted and fit according to eq 1 for (A) dark brown iridal stroma melanosomes and (B) blue-green iridal stroma melanosomes.

generated by the FEL. The data acquired from individual melanosomes identified in the PEEM images were best fit by a single-component equation (eq 1), resulting in a photoionization threshold of 4.9 ± 0.2 eV (253 nm) for both colored iridal stroma melanosomes (Figure 3). The threshold potential for pheomelanin from red hair melanosomes was determined to be 3.8 ± 0.2 eV (326 nm).²⁰ Eumelanosomes exhibit threshold potentials from 4.4 to 4.8 (± 0.2) eV depending on their source (sepia, human hair, bovine, and human RPE).^{14,17,20,25,26} We were unable to obtain images for either dark brown or blue-green iridal stroma melanosomes for wavelengths of light lower than the upper end of the range of threshold values for eumelanin samples, clearly indicating the absence of pheomelanin on, or near, the surface of the melanosome.

Morphological Surface Organization of Iridal Stroma Melanosomes. AFM imaging was used to analyze the morphological organization of iridal stroma melanosomes. Figure 4 reveals the height and phase AFM images for dark brown iridal stroma melanosomes. In these images, a substructure of the melanosome is observed. The melanosome appears to be comprised of a smaller substructure. Such building blocks have been previously reported on several naturally occurring pigments, melanin isolated from the ink sac of the cuttlefish *Sepia officinalis*,³² melanosomes isolated from human black and red hair,³⁵ melanosomes isolated from bovine eyes,²⁸ and melanosomes isolated from the retinal pigment epithelium in human eyes.³⁶

Discussion

Shape and Size Analysis of Iridal Stroma Melanosomes. During the sample preparation, the iridal pigment epithelium (IPE) is carefully removed from the posterior surface of the iris. However, complete dissection of the IPE is nearly impossible to achieve, and the anterior IPE remains tightly bound to the iris tissue.²⁷ As a consequence, melanosomes isolated from this "IPE-scraped" iris tissue comprise those from anterior IPE and iridal stroma. Morphologically, the IPE melanosomes are spherical, with an average diameter of 1.02 μm , whereas the iridal stroma melanosomes are smaller, ovoid-shaped organelles with width and length dimensions of 0.25 and 0.64 μm ,

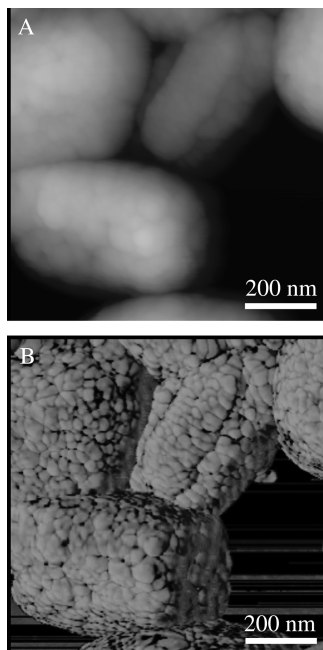


Figure 4. AFM images of dark brown iridal stroma melanosomes. The small substructures of the iridal stroma melanosomes are observed in both images. A is a height image, and B is a phase image.

respectively.^{33,34} To provide insight into the distribution of the isolated melanosomes, a statistical size and shape analysis of the SEM images was conducted. The results revealed a morphology that is consistent with previously reported dimensions for iridal stroma melanosomes (Figure 2). Additionally, the representative SEM images shown in Figure 1 illustrate the dominance of ovoid shapes rather than larger spheres. From the size and shape analysis of the melanosomes isolated from the blue–green and dark brown irides, we confirm that our samples are dominated by iridal stroma melanosomes rather than anterior IPE.

Surface Photoionization Potentials of Iridal Stroma Melanosomes. Melanosomes isolated from the iridal stroma tissue contain both eumelanin and pheomelanin, and the amount and type of melanin present varies with iris color.^{3,27} Despite this fact, an analysis of the plots generated with the FEL-PEEM technique for dark brown and blue–green iridal stroma melanosomes revealed data that was best fit by a single photoionization threshold of 4.9 ± 0.2 eV (253 nm) (Figure 3). This threshold was attributed to eumelanin since it is comparable to the eumelanin threshold established in previous reports on purely eumelanin systems (e.g., sepia ink and black hair melanosomes).^{20,37} For reference, the pheomelanin threshold is characterized as 3.8 ± 0.2 eV (326 nm) from comparison studies on red hair melanosomes.²⁰

PEEM is inherently a surface technique with electrons originating from no further than within a few nanometers of the sample, as estimated for organic structures.³⁸ Melanosomes, however, are effective electron scavengers, and it is likely that the observed image is dominated by the ionization properties of the surface as the electrons generated below are presumed to be efficiently trapped. These results suggest that despite the color origin of the melanosome, only eumelanin components are present on or near the surface. Consistent with this conclusion is our inability to obtain PEEM images on iridal stroma melanosomes using a wavelength that clearly photoionizes pheomelanin in red hair melanosomes.

Morphological Surface Organization of Iridal Stroma Melanosomes.

A more detailed view of the surface of the melanosomes is obtained with the AFM images (Figure 4). These images reveal that the surface of the iridal stroma melanosomes is comprised of smaller substructures. This result was expected based on previous studies of naturally occurring pigments isolated from various sources.^{28,32,35,36} All of the pigments reveal smaller substructures with lateral dimensions of a few tens of nanometers. These results are additionally consistent with the view of melanogenesis proposed by Brumbaugh in the late 1960s.³⁹ In that report, Brumbaugh showed that eumelanin premelanosomes comprise zigzagging longitudinal strands with cross-links that occur every 200 Å. Further analysis of the electron micrographs during the final stages of melanogenesis revealed melanin deposition occurring around and upon these matrixes. As a result of the studies, the FEL-PEEM technique would be probing the surface of these smaller substructures along the surface. Thus, we can conclude that these substructures found along the surface of the iridal stroma melanosomes all have eumelanin coats.

Kinetic studies of the initial steps of the Raper–Mason scheme for melanogenesis established the branching between eumelanin and pheomelanin production. Although initiation of the formation of each pigment is achieved by the enzymatic oxidation of tyrosine by tyrosinase, the kinetic data suggests a three-step process for melanogenesis following this oxidation.^{8,10,11} First, the initial production of cysteinyl-dopa occurs when the cysteine concentration is greater than $1.3 \mu\text{M}$. Then, when the cysteinyl-dopa concentration is greater than $9 \mu\text{M}$, subsequent oxidation of cysteinyl-dopa to pheomelanin occurs. It is only after the depletion of most of the cysteinyl-dopa and cysteine levels that eumelanin formation occurs. These kinetic results suggest a structural design with a pheomelanin core encased by a eumelanin exterior. Studies on the biochemistry of mixed melanogenesis¹³ and the solubility properties of synthetic model systems¹² also proposed this bimolecular casing model. As both of the colored iridal stroma melanosomes analyzed displayed characteristics of pure eumelanin on the surface, our results provide strong evidence for the casing model in human iridal stroma melanosomes.

A chemical analysis investigating the relationship between the amount and type of melanin and iris pigmentation was recently described in the literature.^{3,27} For different colored irides, the amount of pheomelanin remained fairly constant, while the eumelanin component increased in darker-colored irides. As result of the casing model and our FEL-PEEM results, the presence of a relatively constant pheomelanin “core” with a varying eumelanin exterior is proposed for colored iridal stroma melanosomes. The variation of the thickness of the eumelanin shell is attributed to the difference of the eumelanin/pheomelanin ratio. In lighter-colored irides (blue, hazel, etc.), melanosomes have a low eumelanin/pheomelanin ratio, and subsequently, a thin eumelanin shell is expected. On the other hand, darker-colored irides, which possess significantly higher eumelanin/pheomelanin ratios, are expected to have a thick eumelanin exterior.

From the report published recently by Wakamatsu et al., the eumelanin/pheomelanin ratios for uveal melanocytes from eyes with blue–green (hazel) and dark brown irides are identified as 1.3 and 14.8, respectively.³ Using these ratios, conclusions can be drawn about the variation of the thickness of the eumelanin coats. Specifically, calculations show that the eumelanin exterior is 2.48 times thicker for dark brown irides than that for hazel irides, assuming the density of the subunits remains

constant for both colors. If we model the substructure of the melanosomes as spheres of diameter 30 nm, the eumelanin exterior would be ~ 9 and 3.6 nm thick for the dark brown and blue–green iridal melanosome, respectively, and the corresponding diameter of the pheomelanin cores would be ~ 12 and 22.8 nm, respectively. As mentioned, the electron escape depth for melanosomes is expected to be a few nanometers; thus, the absence of the pheomelanin signature is not surprising despite the thin eumelanin shell.

The photoreactivity of the melanin pigment within the melanosome becomes important as a consequence of these results. A dark-colored iris with lower relative pheomelanin concentration (high eumelanin/pheomelanin ratio) is presumed to have a thick eumelanin exterior. Therefore, after the oxidation of the surface pigment, there is still a large amount of eumelanin that can be protective against oxidative stress. However, in melanosomes from light-colored irides, after the oxidation and degradation of the eumelanin surface, a certain amount of pheomelanin molecules are exposed and show their pro-oxidant properties, causing tissue damage. These results are consistent with the incidence of uveal melanoma in different races and in eyes from different colored irides. Epidemiological studies on the relationship between iridal color and incidence of uveal melanoma suggest that the light-colored eye (blue, hazel, etc.) and Caucasian is at a higher risk than the dark-colored eye and African–Asians.^{40–45} Subsequent exposure of the photoreactive and pro-oxidant pheomelanin coupled to the lower total amount of melanin in lighter-colored irides could be a contributor to the observed epidemiology of uveal melanoma.

It is interesting to consider the potential implications of these findings. While we have focused on ocular melanosomes in this paper, we have previously established that a similar encapsulation of pheomelanin by eumelanin pigments is characteristic of the neuromelanin granules isolated from various regions of the human brain.^{14,15,46} This suggests that the structure of melanosomes containing both classes of pigments may share a common structural morphology, independent of tissue type. A recent study on the eumelanin and pheomelanin content in uveal melanoma cells found that melanoma cells have a very low eumelanin content and eumelanin/pheomelanin ratio, significantly lower than that from normal melanocytes. These differences likely render melanoma cells more susceptible to mutagenic effects of UV radiation and oxidative stress and may enhance their proliferation, thereby accelerating the progression of melanoma.⁴⁷ Epidemiological studies indicate that the incidence of cutaneous melanoma in individuals with light-colored skin is greater than that from individuals with dark-colored skin. The relative risk of white/black varies from 12.6 to 17.1 in different reports.^{48–50} Studies of eumelanin and pheomelanin content of epidermal melanocytes from different donors indicate that the eumelanin/pheomelanin ratio correlates with the color of the skin and the ethnic background of the donors. Melanocytes from dark-colored skin and African–American donors have a greater amount of eumelanin and a high ratio of eumelanin/pheomelanin as compared to that with lighter-colored skin and Caucasian.⁵¹ If the melanosomes in uveal melanoma cells and epidermal melanocytes have a similar structure as that in iridal melanocytes melanosomes, the different incidence of cutaneous melanoma in individuals with various colored skins and the progress of uveal melanoma could be explained, at least partly, by the structure of melanosomes and the different thicknesses of eumelanin coats.

Conclusion

The surface potentials of iridal stroma melanosomes from human dark brown and blue–green irides have been studied with FEL-PEEM, and further analysis of the surface morphology was probed with AFM. All melanosomes show pure eumelanin on their surfaces, independent of their respective eumelanin/pheomelanin ratios. These results provide very strong evidence for the casing model in the human irides and imply that the smaller substructures all have eumelanin coats of varying thickness. This result provides new insights into the molecular mechanisms underlying the epidemiology of uveal melanoma. As the reactive pheomelanin is encased by the photoprotective eumelanin, degradation of the eumelanin exterior is necessary to expose the pro-oxidant, photoreactive properties of the pheomelanin core. Degradation of the eumelanin surface can be achieved through several processes (photobleaching, oxidation), but exposure of the pheomelanin core will result more quickly in lighter-colored irides with thinner eumelanin shells. These results are consistent with the epidemiological studies, which show that the incidence of uveal melanomas is greater in Caucasian and in eyes with light-colored irides. Further studies are needed, however, to confirm that the outer protective layer thins with the lightening of the color of the iris.

Acknowledgment. This research was supported by Duke University. D.N.P. is grateful for the support of the Paul M. Gross Fellowship. We thank Calvin Howell of TUNL for providing the FEL time needed to conduct these experiments.

References and Notes

- Wakamatsu, K.; Kavanagh, R.; Kadekaro, A. L.; Terzieva, S.; Sturm, R. A.; Leachman, S.; Abdel-Malek, Z.; Ito, S. *Pigm. Cell Res.* **2006**, *19*, 154.
- Ito, S.; Wakamatsu, K. *Pigm. Cell Res.* **2003**, *16*, 523.
- Wakamatsu, K.; Hu, D.-N.; McCormick, S. A.; Ito, S. *Pigment Cell Melanoma Res.* **2007**, *21*, 97.
- Hu, D.-N.; Simon, J. D.; Sarna, T. *Photochem. Photobiol.* **2008**, *84*, 639.
- Wenczl, E.; Schans, G. P. V. d.; Roza, L.; Kolb, R. M.; Timmerman, A. J.; Smit, N. P. M.; Pavel, S.; Schothorst, A. A. *J. Invest. Dermatol.* **1998**, *111*, 678.
- Vincensi, M. R.; d'Ischia, M.; Napolitano, A.; Procaccini, E. M.; Riccio, G.; Monfrecola, G.; Santolanni, P.; Prota, G. *Melanoma Res.* **1998**, *8*, 53.
- Boissy, R. E.; Hornyak, T. J. *Extracutaneous Melanocytes. In The Pigmentary System: Physiology and Pathology*, 2nd ed.; Nordlund, J. J., Boissy, R. E., Hearing, V. J., King, R. A., Oetting, W. S., Ortonne, J.-P., Eds.; Blackwell Publishing: Cambridge, MA, 2006; p 91.
- Ito, S.; Wakamatsu, K. *Photochem. Photobiol.* **2008**, *84*, 582.
- Land, E. J.; Ito, S.; Wakamatsu, K.; Riley, P. A. *Pigm. Cell Res.* **2003**, *16*, 487.
- Land, E. J.; Riley, P. A. *Pigm. Cell Res.* **2000**, *13*, 273.
- Ito, S. *Pigm. Cell Res.* **2003**, *16*, 230.
- Ozeki, H.; Ito, S.; Wakamatsu, K.; Ishiguro, I. *Biochim. Biophys. Acta* **1997**, *1336*, 539.
- Agrup, G.; Hansson, C.; Rorsman, H.; Rosengren, E. *Arch. Dermatol. Res.* **1983**, *272*, 103.
- Bush, W. D.; Garguilo, J.; Zucca, F. A.; Albertini, A.; Zecca, L.; Edwards, G. S.; Nemanich, R. J.; Simon, J. D. *Proc. Natl. Acad. Sci. U.S.A.* **2006**, *103*, 14785.
- Ito, S. *Proc. Natl. Acad. Sci. U.S.A.* **2006**, *103*, 14647.
- Wakamatsu, K.; Fujikawa, K.; Zucca, F. A.; Zecca, L.; Ito, S. *J. Neurochem.* **2003**, *86*, 1015.
- Simon, J. D.; Hong, L.; Peles, D. N. *J. Phys. Chem. B* **2008**, *112*, 13201.
- Hill, H. Z. *BioEssays* **1992**, *14*, 49.
- Sarna, T.; Menon, I. A.; Sealy, R. C. *Photochem. Photobiol.* **1984**, *39*, 805.
- Ye, T.; Hong, L.; Garguilo, J.; Pawlak, A.; Edwards, G. S.; Nemanich, R. J.; Sarna, T.; Simon, J. D. *Photochem. Photobiol.* **2006**, *82*, 733.
- Takeuchi, S.; Zhang, W.; Wakamatsu, K.; Ito, S.; Hearing, V. J.; Kraemer, K. H.; Brash, D. E. *Proc. Natl. Acad. Sci. U.S.A.* **2004**, *101*, 15076.

- (22) Persad, S.; Menon, I. A.; Haberman, H. F. *Photochem. Photobiol.* **1983**, *37*, 63.
- (23) Harsanyi, Z. P.; Post, P. W.; Brinkmann, J. P.; Chedekel, M. R.; Deibel, R. M. *Experientia* **1980**, *36*, 291.
- (24) Chedekel, M. R.; Smith, S. K.; Post, P. W.; Pokora, A.; Vessell, D. L. *Proc. Natl. Acad. Sci. U.S.A.* **1978**, *75*, 5395.
- (25) Samokhvalov, A.; Hong, L.; Liu, Y.; Garguilo, J.; Nemanich, R. J.; Edwards, G. S.; Simon, J. D. *Photochem. Photobiol.* **2005**, *81*, 145.
- (26) Samokhvalov, A.; Garguilo, J.; Yang, W.-C.; Edwards, G. S.; Nemanich, R. J.; Simon, J. D. *J. Phys. Chem. B* **2004**, *108*, 16334.
- (27) Prota, G.; Hu, D.-N.; Vincensi, M. R.; McCormick, S. A.; Napolitano, A. *Exp. Eye Res.* **1998**, *67*, 293.
- (28) Liu, Y.; Hong, L.; Wakamatsu, K.; Ito, S.; Adhyaru, B. B.; Cheng, C.-Y.; Bowers, C. R.; Simon, J. D. *Photochem. Photobiol.* **2005**, *81*, 510.
- (29) Ade, H.; Yang, W.; English, S. L.; Hartman, J.; Davis, R. F.; Nemanich, R. J.; Litvinenko, V. N.; Pinayev, L. V.; Wu, Y.; Madey, J. M. *J. Surf. Rev. Lett.* **1998**, *5*, 1257.
- (30) Senturia, S. D. *Microsystem Design*; Kluwer Academic Publishers: Boston, MA, 2001; p 34.
- (31) Fowler, R. H. *Phys. Rev.* **1931**, *38*, 45.
- (32) Clancy, C. M. R.; Simon, J. D. *Biochemistry* **2001**, *40*, 13353.
- (33) Hu, D.-N.; McCormick, S. A.; Ritch, R.; Pelton-Henrion, K. *Invest. Ophthalmol. Visual Sci.* **1993**, *34*, 2210.
- (34) Hu, D.-N.; Ritch, R.; McCormick, S. A.; Pelton-Henrion, K. *Invest. Ophthalmol. Visual Sci.* **1992**, *33*, 2443.
- (35) Liu, Y.; Hong, L.; Wakamatsu, K.; Ito, S.; Adhyaru, S.; Cheng, C.-Y.; Bowers, C. R.; Simon, J. D. *Photochem. Photobiol.* **2005**, *81*, 135.
- (36) Hong, L.; Garguilo, J.; Anzaldi, L.; Edwards, G. S.; Nemanich, R. J.; Simon, J. D. *Photochem. Photobiol.* **2006**, *82*, 1475.
- (37) Garguilo, J.; Hong, L.; Edwards, G. S.; Nemanich, R. J.; Simon, J. D. *Photochem. Photobiol.* **2007**, *83*, 692.
- (38) Houle, W. A.; Engel, W.; Willig, F.; Rempfer, G. F.; Griffith, O. H. *Ultramicroscopy* **1982**, *7*, 371.
- (39) Brumbaugh, J. A. *Dev. Biol.* **1968**, *18*, 375.
- (40) Hu, D.-N.; Yu, G.-P.; McCormick, S. A.; Schneider, S.; Finger, P. T. *Am. J. Ophthalmol.* **2005**, *140*, 612.
- (41) Vajdic, C. M.; Krickler, A.; Giblin, M.; McKenzie, J.; Aitken, J.; Giles, G. G.; Armstrong, B. K. *Int. J. Cancer* **2001**, *92*, 906.
- (42) Seddon, J. M.; Gragoudas, E. S.; Glynn, R. J.; Egan, K. M.; Albert, D. M.; Blitzer, P. H. *Arch. Ophthalmol.* **1990**, *108*, 1274.
- (43) Holly, E. A.; Aston, D. A.; Char, D. H.; Kristiansen, J. J.; Ahn, D. K. *Cancer Res.* **1990**, *50*, 5773.
- (44) Tucker, M. A.; Shields, J. A.; Hartge, P.; Augsburger, J.; Hoover, R. N.; Fraumeni, J. F. *N. Engl. J. Med.* **1985**, *313*, 789.
- (45) Michelson, J. B.; Shields, J. A. *Am. J. Ophthalmol.* **1977**, *83*, 694.
- (46) Bush, W. D.; Garguilo, J.; Zucca, F. A.; Bellei, C.; Nemanich, R. J.; Edwards, G. S.; Zecca, L.; Simon, J. D. *Photochem. Photobiol.* **2009**, *85*, 387.
- (47) Hu, D.-N.; Wakamatsu, K.; Ito, S.; McCormick, S. A. *Melanoma Res.* **2009**, *19*, 75.
- (48) Tsai, T.; Vu, C.; Henson, D. E. *Melanoma Res.* **2005**, *15*, 213.
- (49) Cress, R. D.; Holly, E. A. *Cancer, Causes Control, Pap. Symp.* **1997**, *8*, 246.
- (50) Neugut, A. I.; Kizelnik-Freilich, S.; Ackerman, C. *Am. J. Public Health* **1994**, *84*, 1828.
- (51) Wakamatsu, K.; Kavanagh, R.; Kadekaro, A. L.; Terzieva, S.; Strum, R. A.; Leachman, S.; Abdel-Malek, Z.; Ito, S. *Pigm. Cell Res.* **2006**, *29*, 154.

JP904138N